Robotica (1997) volume 15, pp 225–231. © 1997 Cambridge University Press

Modelling of a camera-3D range finder system

Christian Barat, Jean Triboulet, Youcef Chekhar, and Etienne Colle

CEMIF Systèmes Complexes, 40 Rue du Pelvoux 91 020 Evry Cedex (France)

(Received in Final Form: May 18, 1996)

SUMMARY

A laser range finder mounted on a site and azimuth turret is used as a 3D range camera. It forms, associated with a video camera, an original stereovision system. The internal structure of both images are the same but the resolution of 3D image stays low. By ignoring the acquiring speed of measures, spatial resolution is limited by the accuracy of deviation device and the laser footprint. The fact that the impact of the beam is not a point introduces spatial integration.

To correct the average at depth discontinuities due to the beam footprint, a neural-network-based solution is reported.

The use of such a multisensor system requires its calibration. As camera calibration is a well-known problem, the paper focuses on models and calibration methods of the range finder. Experimental results illustrate the quality of the calibration step in terms of accuracy and stability.

The footprint correction is evaluated for both 1D and 2D range finder scannings.

KEYWORDS: 3D range finder; Modelling; Camera; Calibration.

1. INTRODUCTION

The geometric modelling of the environment can be carried out using a stereovision system. But in the case of a degraded image due to vision conditions, robustness and accuracy in depth measures are poor. If one of the video cameras is replaced by a range image device, the advantages of each sensor can be combined to increase the quality and the complexity of data.

A range system generates a range image where each pixel represents a depth. But, although the internal structure of a video camera and range image are the same, the latter presents poor resolution which poses a problem during the matching step.

In the first section, we present the problem of multisensor calibration. Measurements have to be translated relatively to the same reference frame.

The camera calibration is now a well-known problem; we focus on the geometric model of the range finder and methods we studied to determine it. Experimental results allow the evaluation of several models and methods in terms of accuracy and stability.

In the second section, the building of a 3D image is studied. Its spatial resolution depends on two factors: the angular accuracy of the rotation device, on which the range finder is mounted, and the diameter of the laser beam which increases with the depth of the target. We put the stress on the latter point responsible for the so-called ''footprint''. During scanning, the beam operates as a spatial filter and any depth discontinuity is averaged with neighbour points. (See references 1 and 2 where the problem is quoted without correcting it, so the scanning step is limited according to the size of the laser impact).

We propose a neural-network-based solution to improve the spatial resolution, which acts as an ''inverse model''. The aimed application consists of a perceptual aid for an operator in teleoperation. In case of indirect viewing via a video camera, the 3D image is superimposed onto the video image to provide the operator with a better perception of depth. This is a typically enhanced reality.

Such an application does not directly concern the geometric modelling of environment, but requires the same matching step.

2. MULTISENSOR CALIBRATION

The geometric sensor model defines the transformation from one frame (source) to another (destination). The sensor calibration determines the parameters of the transformtion with the help of special points called ''calibration points''. Their coordinates are known in source and destination frames. We first present briefly a camera calibration method, then we detail two methods for range finder calibration.

2.1. Camera calibration

The camera model C is defined by the relationship between the homogeneous coordinates of a point $M(x_o, y_o, z_o, 1)^t$, relative to the world coordinate frame R_o, and its image $m(u, v)^t$ in pixels (Fig. 1).

A pin-hole model describes the optical part of the video camera, so:

$$\begin{pmatrix} u \cdot s \\ v \cdot s \\ s \end{pmatrix} = C \cdot \begin{pmatrix} x_o \\ y_o \\ z_o \\ 1 \end{pmatrix} \quad (1)$$

The resolution of the model, *i.e.* the estimation of matrix

https://doi.org/10.1017/S0263574797000246 Published online by Cambridge University Press

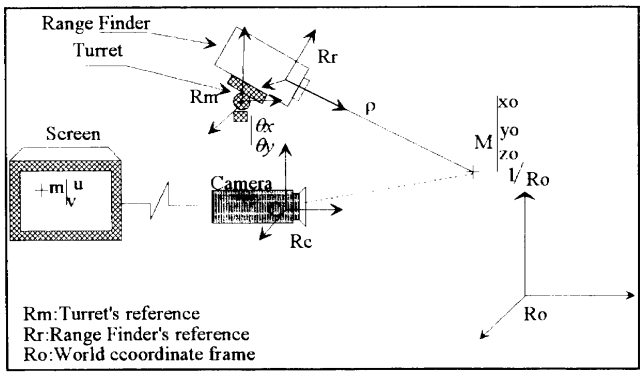

Fig. 1. Multisensor system and coordinate frames.

coefficients, has been carried out using extented Kalman filter. Complete results are presented in reference 3.

2.2. *Range finder calibration*

Two calibration methods are studied:

- The first one uses a Least Square resolution and constraint propagation on the geometric particularities of the model.
- The second one is based on an optimisation technique and allows the determination of parameters in case of a non-linear model. In the following, internal and external models of the range finder are distinguished.

2.2.1. Modelisation. Let Rr be the range finder-related frame (see Figure 1).

The homogeneous coordinates of M, expressed in Rr, are $(0, 0, -\rho, 1)^t$. The range finder is mounted on a two-degrees-of-freedom turret swivelling according to sight and azimuth angles θ_x and θ_y. The geometric model of this device is a 4×4 homogeneous matrix M_{glob} defining the coordinate transformation between Ro and Rr:

$$\begin{pmatrix} x_o \\ y_o \\ z_o \\ 1 \end{pmatrix} = M_{glob} \cdot \begin{pmatrix} 0 \\ 0 \\ -\rho \\ 1 \end{pmatrix} \tag{2}$$

This global model of the range finder can be divided into internal and external models (see Figure 2).

(i) *Internal model of the range finder.* The internal model depends on the device structure. It is a 4×4 homogeneous matrix M_{Int} defining the coordinates

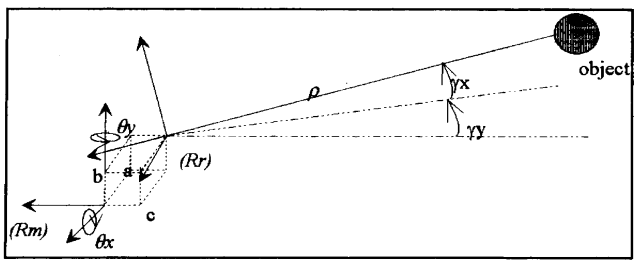

Fig. 2. Range finder frames.

transformation between Rm, attached to the turret base, and the range finder frame Rr:

$$\begin{pmatrix} x_m \\ y_m \\ z_m \\ 1 \end{pmatrix} = M_{Int} \cdot \begin{pmatrix} 0 \\ 0 \\ -\rho \\ 1 \end{pmatrix} \tag{3}$$

The transformation depends on the nature of the mechanical link between the range finder and the turret and expresses the two frames coincidence defaults.

According to the mechanical structure of the device, M_{Int} is given by the following relation:

$$M_{Int} = \begin{pmatrix} R_{(\theta_x,\theta_y)} & 0 \\ 0 & 1 \end{pmatrix} \cdot \begin{pmatrix} 1 & T_{(a,b,c)} \\ 0 & 1 \end{pmatrix} \cdot \begin{pmatrix} R_{(\gamma_x,\gamma_y} & 0 \\ 0 & 1 \end{pmatrix} \tag{4}$$

where $\mathbf{R}(\gamma_x, \gamma_y)$ and $\mathbf{T}(a, b, c)$ are the rotation and translation sub-matrices correcting frame coincidence defaults respectively.

$\mathbf{R}(\theta_x, \theta_y)$ represents the rotation angles of turret's motors.

(ii) *External model of the range finder.* The external model is the 4×4 homogeneous matrix defining the coordinates transformation from Rm to Ro:

$$\begin{pmatrix} x_o \\ y_o \\ z_o \\ 1 \end{pmatrix} = M_{Ext} \cdot \begin{pmatrix} x_m \\ y_m \\ z_m \\ 1 \end{pmatrix} \tag{5}$$

2.2.2. Calibration. Two approaches are presented in the following section:

The first one determines M_{int} and M_{ext}. The second one identifies directly the global model M_{glob}.

(i) *First calibration approach.* In this case, the internal model is defined with a, b, c parameters from mechanical dimensions given by the manufacturer. γ_x and γ_y; the adjustment angles, have been obtained by an experimental procedure using a mirror as a target and an autocollimation technique.

$$\begin{cases} a = 0.5 \pm 0.01 \text{ mm}; \quad b = c = 0 \pm 0.01 \text{ mm} \\ \gamma_x = -1.15 \pm 0.05°; \quad \gamma_y = -0.23 \pm 0.05° \end{cases} \tag{6}$$

Two ways are possible following the formalism of the model. A constraint propagation method applied to the homogeneous-matrix formalism has been tested in reference 4.

Another way consists of using the Rodrigues' formalism which leads to a more concise expression of the rotation. The translation between the two frames is expressed by a 3 components vector.

As seen just before, only the external model is given. The method determines the rotation parameters and the translation vector by a least square criterion.

Using Rodrigues' formalism, let vector $\vec{v}_i'$ deduced from $\vec{v}_i$ by rotation of matrix $\mathbf{R}$, be

$$\vec{v}_i' = R \cdot \vec{v}_i$$

https://doi.org/10.1017/S0263574797000246 Published online by Cambridge University Press

and

$$\underset{R}{\text{Min}}\left(\sum_{i=1}^{N}\|\vec{v}_i' - R\cdot\vec{v}_i\|^2\right) \tag{7}$$

expresses the optimal rotation of a N measurements system (vector $\vec{v}_i'$ and $\vec{v}_i$ are defined from Rm and Ro frames).

The rotation vector gives a representation with only four parameters:

$\vec{n} = (n_x, n_y, n_z)^t$ represents the rotation vector

α represents the rotation angle around the axis defined by $\vec{n}$.

With Rodridgues' relation:

$$\vec{v}_i' = \vec{v}_i + (\vec{n}\wedge\vec{v}_i)\cdot\sin(\alpha) + \vec{n}\wedge(\vec{n}\wedge\vec{v}_i)\cdot(1-\cos(\alpha))$$

Each measurement i leads to a three equations system:

$$\vec{v}_i' - \vec{v}_i = s(\vec{v}_i' + \vec{v}_i)\cdot\vec{u}$$

where:

$$\vec{u} = (u_x, u_y, u_z)^t \quad \text{is defined as } \vec{u} = \tan\left(\frac{\alpha}{2}\right)\cdot\vec{n}$$

$s(\vec{v}_i' + \vec{v}_i)$ is the antisymmetrical cross product matrix of vector $(\vec{v}_i' + \vec{v}_i)$, the rank of s is 2.

If N points are available the system is composed of $2N$ independent equations. In a matrix form:

$$\mathbf{Y} = \mathbf{H}\cdot\mathbf{u} \tag{8}$$

with:

$$H = \begin{pmatrix} 0 & -(v_{z_1}' + v_{z_1}) & (v_{y_1}' + v_{y_1}) \\ (v_{z_1}' + v_{z_1}) & 0 & -(v_{x_1}' + v_{x_1}) \\ — & — & — \\ — & — & — \\ 0 & -(v_{z_N}' + v_{z_N}) & (v_{y_N}' + v_{y_N}) \\ (v_{z_N}' + v_{z_N}) & 0 & -(v_{x_N}' + v_{x_N}) \end{pmatrix}$$

$$Y = \begin{pmatrix} (v_{x_1} - v_{x_1}') \\ (v_{y_1} - v_{y_1}') \\ — \\ — \\ (v_{x_N} - v_{x_N}') \\ (v_{y_N} - v_{y_N}') \end{pmatrix} \quad \vec{u} = \begin{pmatrix} u_x \\ u_y \\ u_z \end{pmatrix}$$

The optimal solution is obtained applying a mean square method:

$$\vec{u} = (H^t\cdot H)^{-1}\cdot H^t\cdot Y \tag{9}$$

This, finally, leads to:

$$\vec{n} = \frac{\vec{u}}{\|\vec{u}\|} \tag{10}$$

and

$$\alpha = 2\cdot\arctan(\|\vec{u}\|) \tag{11}$$

If required, the rotation matrix R can be expressed as a function of $\vec{n}$ and α:

$$R = \cos(\alpha)\cdot Id + (\vec{n}\cdot\vec{n})\cdot(1-\cos(\alpha)) + s(\vec{n})\cdot\sin(\alpha) \tag{12}$$

$s(\vec{n})$ is the antisymmetrical cross-product matrix related to vector $\vec{n}$.

Let $\cos(\alpha) = c$ and $\sin(\alpha) = s$, then R can be expressed by:

$$\begin{pmatrix} c + (1-c)\cdot n_x^2 & (1-c)\cdot n_x\cdot n_y - s\cdot n_z & (1-c)\cdot n_x\cdot n_z + s\cdot n_y \\ (1-c)\cdot n_x\cdot n_y + s\cdot n_z & c + (1-c)\cdot n_y^2 & (1-c)\cdot n_z\cdot n_y - s\cdot n_x \\ (1-c)\cdot n_x\cdot n_z - s\cdot n_y & (1-c)\cdot n_z\cdot n_y + s\cdot n_x & c + (1-c)\cdot n_z^2 \end{pmatrix} \tag{13}$$

The translation sub-matrix is obtained by the relation:

$$T = B' - R\cdot B \tag{14}$$

where:

$$B = \frac{1}{N}\sum_{i=1}^{N} P_i \quad B' = \frac{1}{N}\sum_{i=1}^{N} P_i'$$

P_i and P_i' represents calibration points.

(ii) *Second calibration approach.* The Levenberg & Marquardt optimisation method (see reference 5) allows the determination of both internal and external models of the range finder.

Internal model

Taking into account the mechanical structure (see equation (4)) internal model is expressed as:

$$\begin{cases} x_m = -\rho\cdot(-\gamma_y\cdot c\theta_y + \gamma_x\cdot s\theta_x\cdot s\theta_y - c\theta_x\cdot s\theta_y) \\ \qquad + a_{ir}\cdot c\theta_y + b_{ir}\cdot s\theta_x\cdot s\theta_y - c_{ir}\cdot c\theta_x\cdot s\theta_y \\ y_m = -\rho\cdot(\gamma_x\cdot c\theta_x + s\theta_x) + b_{ir}\cdot c\theta_x + c_{ir}\cdot s\theta_x \\ z_m = -\rho\cdot(-\gamma_y\cdot s\theta_y - \gamma_x\cdot s\theta_x\cdot c\theta_y + c\theta_x\cdot c\theta_y) \\ \qquad + a_{ir}\cdot s\theta_y - b_{ir}\cdot s\theta_x\cdot c\theta_y + c_{ir}\cdot c\theta_x\cdot c\theta_y \end{cases} \tag{15}$$

External model

The external model is a homogeneous matrix:

$$M_{Ext} = \begin{pmatrix} R_{(\alpha,\vec{n})} & T \\ 0 & 1 \end{pmatrix} \tag{16}$$

where R and T are rotation and translation submatrices.

Global model

This representation leads to three equations used to determine the criterion:

$$M_{Glob} = M_{Ext}\cdot M_{Int} \tag{17}$$

where:

$$\begin{pmatrix} x_o \\ y_o \\ z_o \\ 1 \end{pmatrix} = M_{GLob}\cdot\begin{pmatrix} 0 \\ 0 \\ -\rho \\ 1 \end{pmatrix} \tag{18}$$

and

$$\begin{cases} x_o = -\rho\cdot M_{Glob[1,3]} + M_{Glob[1,4]} \\ y_o = -\rho\cdot M_{Glob[2,3]} + M_{Glob[2,4]} \\ z_o = -\rho\cdot M_{Glob[3,3]} + M_{Glob[3,4]} \end{cases} \tag{19}$$

The optimisation process minimises a mean square

https://doi.org/10.1017/S0263574797000246 Published online by Cambridge University Press

criterion (19), taking into account the rotation vector norm.

$$Crit = \sum_{i=1}^{N} \begin{bmatrix} (x_{o\_i} + \rho_{\_i} \cdot M_{glob[1,3]\_i} - M_{glob[1,4]\_i})^2 \\ + (y_{o\_i} + \rho_{\_i} \cdot M_{Glob[2,3]\_i} - M_{Glob[2,4]\_i})^2 \\ + (z_{o\_i} + \rho_{\_i} \cdot M_{Glob[3,3]\_i} - M_{Glob[3,4]\_i})^2 \\ + (1 - \|\vec{n}\|)^2 \end{bmatrix} \quad (20)$$

The Levenberg-Marquart optimisation is applied twice. In the first step, the internal model is not taken into account, *i.e.* its parameters are taken equal to zero. The solution is an approximation to the external model. It allows the initialisation of the non-linear process carried out in the second step, which solves the global model.

Then in a few steps the algorithm converges to an optimal solution.

2.2.3. Results. (i) *Experimental environment.* The calibration methods need two distinct sets of measurements:

the first set for the calibration step
the second one for the evaluation step

They are made on an experimental stand composed of a mobile carriage following an x and y horizontal plane and a calibration grid.

(ii) *Main characteristics of the experimental site.* The world frame point coordinates are known with a 0.1 mm accuracy.

The carriage translation accuracy is also 0.1 mm.

The range finder has the following characteristics:
—statistical accuracy on distance ρ: 3 mm
—angular accuracy on θ_x and θ_y: 0.01°
—mean distaince range finder/target: 1700 mm.

(iii) *Evaluation elements.* The building error is defined as the difference between coordinates of points known (0.1 mm) in a Ro frame and the coordinates of the same points computed from measurements in a sensor frame and estimated model.

Figure 3 shows tz parameter evolution versus the number of calibration.

Only the tz parameter is presented (worst case). For the first approach, it is more stable than the second one.

Table I shows building errors. Building errors related to range finder/grid distance are about 0.26% on x, 0.15% on y and 0.62% on z for the Least Square method and about 0.15% on x, 0.14% on y and 0.35% on z for the optimisation method.

Thus the optimisation method seems to give the best results.

Table I. Building errors for 25 calibrating points

	$N = 25$ calibration points	Least Square Method	Optimisation Method
Absolute Mean (m)	Mx	9.64E-04	1.00E-03
	My	7.97E-04	6.41E-04
	Mz	5.54E-03	2.73E-03
Standard Deviation (m)	Sx	1.15E-03	7.99E-04
	Sy	1.17E-03	7.46E-04
	Sz	6.32E-03	1.75E-03
Maximum (m)	Ex	2.70E-03	2.64E-03
	Ey	4.42E-03	2.74E-03
	Ez	1.06E-02	5.95E-03

3. FOOTPRINT CORRECTION

3.1. Presentation of the sensing system

Before developing the approaches to correct the footprint error, the sensing system is presented.

To get a depth image of the environment the range-finder scans the scene with constant steps (θ_x, θ_y) (see Figure 4).

3.2. Telemeter characteristics

The sensor is a commercial device of IBEO (reference 6). The distance is computed from the measure of the wave time-of-flight between the target and the sensor. The wave-length of the laser pulse is 905 nm.

Four accuracies, given by the manufacturer as statistical standard deviations, are available: 20, 10, 5, 3 mm.

The main error is the footprint error depending on beam diameter. The beam model (20), proposed in

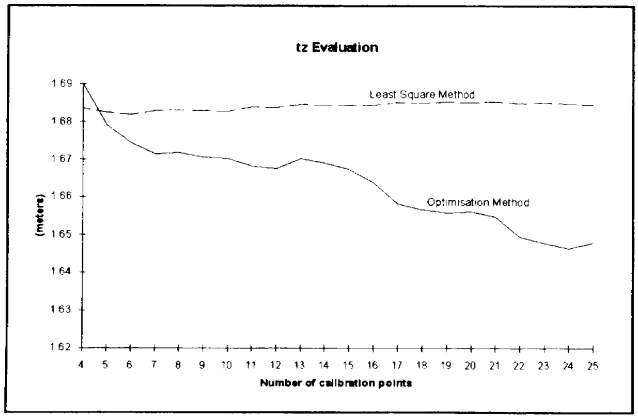

Fig. 3. Variation of tz parameter.

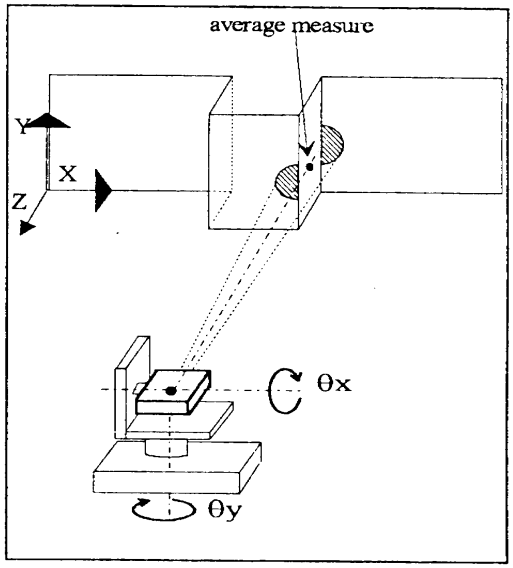

Fig. 4. 3D sensor.

https://doi.org/10.1017/S0263574797000246 Published online by Cambridge University Press

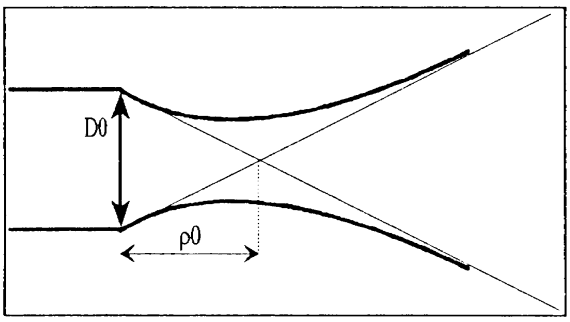

Fig. 5. Beam model

reference 7, is illustrated (see Figure 5). An experimental study for different distances (0.6 to 5 m) has allowed the identification of the sensor model parameters.

$$D^2(\rho) = D_0^2\left(\frac{\rho - \rho_0}{\rho_0}\right)^2 + D_{\min}^2 \qquad (21)$$

lens diameter $D_0 = 14$ mm
waist $D_{\min} = 7$ mm
focusing distance $\rho_0 = 3.1$ m

3.3. Method used to correct the footprint error

Several remarks can be deduced from the study of the physical sensor characteristics:

1. The error of measures (footprint) appears when the laser is scanning a discontinuity of depth. Therefore, this part of profile has to be found and corrected.
2. If the distance between two discontinuities of depth is less than the beam diameter, there is a critical lost of information and no correction seems possible.

The following section describes three approaches to correct the footprint error with the aim of improving the depth image:

a. Parametric Inverse Model
b. Neural Inverse Model
c. Neural-Parametric Inverse Model

3.3.1. Parametric Inverse Model. The telemeter appears as a *black box* which is the parametric model. The telemeter characteristics leads to the Finite Impulse Response (F.I.R.) representation:

$u(k)$ = discrete input
$y(k)$ = discrete output
$H(z^{-1})$ = discrete transfer function
$e(k)$ = discrete white noise ($\sigma = 3$ mm)
$y(k) = H(z^{-1})u(k) + e(k)$ direct model
$u(k) = H^{-1}(z^{-1})(y(k) - e(k))$ inverse model

Due to the beam divergence, an inverse model has to be found, for each distance, to correct measures. The model found for one distance is often unsteady.

3.3.2. Neural Inverse Model. The neural approach appears as another way to determine the inverse model when classical approaches are invalid.[8]

The neural network can be represented as a universal estimator. It is generally modelled by several fully interconnected layers of elements called 'neurons'.

The neural network used is a feedforward network; the information flow is transmitted from layer to layer (from input layer to output layer). The learning algorithm suitable for this kind of problem and network architecture is the backpropagation. This algorithm is summarised below:

1. presentation phase
2. propagation in the network
3. computation of the criteria error
4. backpropagation phase
5. modification of network weights
6. evaluation of the stop criterion

The choice of a neural network architecture for the input number and output number is conducted by the characteristics of the system to design. The number of inputs is constrained by the beam diameter and the step of measure. This network is composed of 1 hidden layer with an output and 6 inputs, with a Sigmoide (non linear) activation function. The entry vector is made of 5 measures $y(k)$ normalised between 0.1 and 0.9, and an indication of the distance $d(k)$ also normlised (0 for 0 m and 1 for 5 m). The output vector is the real distance (see Figure 6).

The size of the hidden layer is a variable depending of each system; there are no rules to determine it. The training uses the Nguyen and Widrow initialisation. To avoid local minima due to the bad initialisation and to select the best architecture, the effects of hidden neurons and initialisations have been tested as compared to the generalization error (see Figure 7). It appears that 8 hidden neurons give the best results.

The improvement of the measure is not satisfying; the error after correction remains too significant. In addition, the neural network has some problems in trying to correct a different class of a discontinuity of depth. It works better for very specialised tasks.

3.3.3. Neural Detection-Parametric Correction

(i) *Presentation*

The principle of the approach described below is to split detection of profile classes and data correction.

(ii) *Detection of classes profile*

The classification is a well adapted task to neural network.[9]

These profiles are classified into 4 classes (see Figure 8):

1. line of slope 0 (order 0)
2. line of constant slope (order 1)
3. curve (order 2)

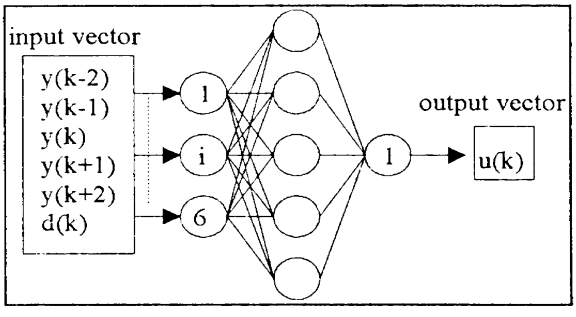

Fig. 6. Neural network.

https://doi.org/10.1017/S0263574797000246 Published online by Cambridge University Press

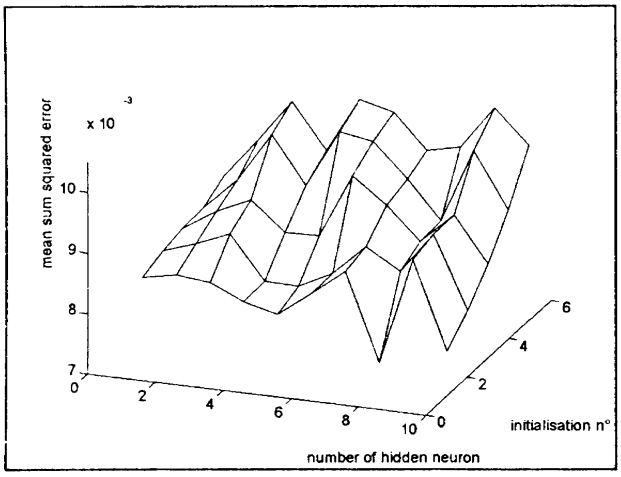

Fig. 7. Surface of error for 50 learning.

4. discontinuity of depth

In the preprocessing step a derivative filter is used to extract features of the profile. One neural network is used for each class to optimise the results of detection. The final choice of class among the four outputs of neural networks is done by the maximal output greater than a threshold value (see Figure 9).

The neural network architecture is different for each detection only at hidden layer level. The choice is made as in the previous paragraph, by comparing different numbers of hidden neurons. The number of discrete inputs and output are, respectively, 5 and 1 (Table II).

The percentages are:

$$d = \frac{\text{number of vectors of good classes detected}}{\text{number of vectors of the class to be detected}}$$

$$\text{ied} = \frac{\text{number of vectors of false classes detected}}{\text{number of vectors not to be detected}}$$

(iii) *Correction of profile*

The different steps of the detection–correction are presented:

1. Measurement (see Figure 10)
2. Detection of profile classes (see Figure 11).
3. Estimation of the discontinuity position (zero crossing of second derivative).
4. Estimation of the coefficients of a polynomial $p(x)$ of degree $n =$ class that fits the data, $p(x(i)) \approx z(i)$, in a least-square sense. The coefficients are computed versus measures, before the discontinuity profile (b) and after (a) in Figure 12.1.
5. Substitution of the discontinuity part by the 2 polynomials extrapolated until the discontinuity position (see Figure 12.2).

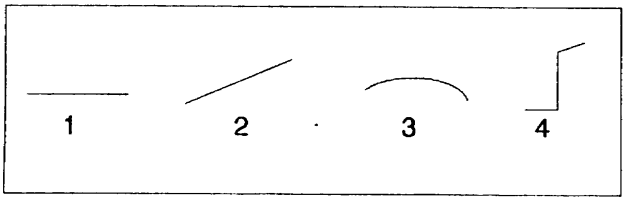

Fig. 8. Classes of profile.

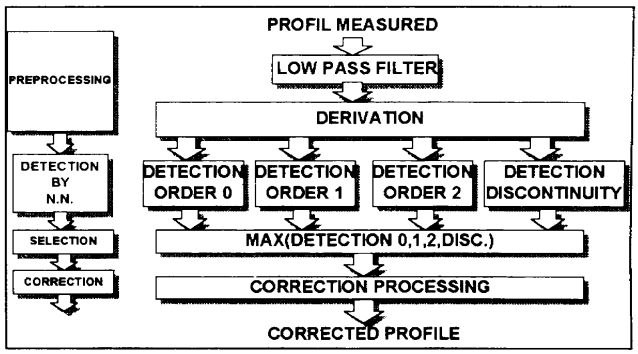

Fig. 9. Detection structure.

3.3.4. Results. The profile (see Figure 13) is composed of three distinct parts: order 1, discontinuity, order 1.

To evaluate the improvement brought by the process, a criterion is computed:

error before correction (ebc):

$$ebc = \frac{\sum_{1}^{n} (y_{real} - y_{measured})^2}{n} \tag{22}$$

error after correction (eac):

$$eac = \frac{\sum_{1}^{n} (y_{real} - y_{corrected})^2}{n} \tag{23}$$

For this representative sample the results are:

$$ebc = 94.5$$
$$eac = 0.95$$

Case of a depth image

The techniques can be spread over a depth image, line by line and column by column.

For a scene (50×217 mm) composed of two cubes ($25 \times 25 \times 50$) and one cylinder ($\phi 60 \times 25$) located at 5 m from the range finder:

$$ebc = 9.587E + 04$$
$$eac = 7.502E + 03$$

The image size is 50×217 pixel.

4. CONCLUSION

The multisensor system is composed of a camera and a 3D range finder.

The calibration step allows one to express the measures of each sensor in the same reference frame. For the camera, it has been carried out using the extended Kalman filter. For the 3D range finder, two approaches based on Rodrigues' formalism are presented. The first one, a least square method, leads to a

Table II. Optimal *NN* structure and detection results

Detection	Structure I-H-O	Detection (d)	Interlcass error detection (ied)
Order 0	5-6-1	93.8%	0.7%
Order 1	5-8-1	79.1%	9%
Order 2	5-6-1	94%	13%
Discontinuity	5-9-1	78%	1.5%

I = input, H = hidden, O = output neurons.

https://doi.org/10.1017/S0263574797000246 Published online by Cambridge University Press

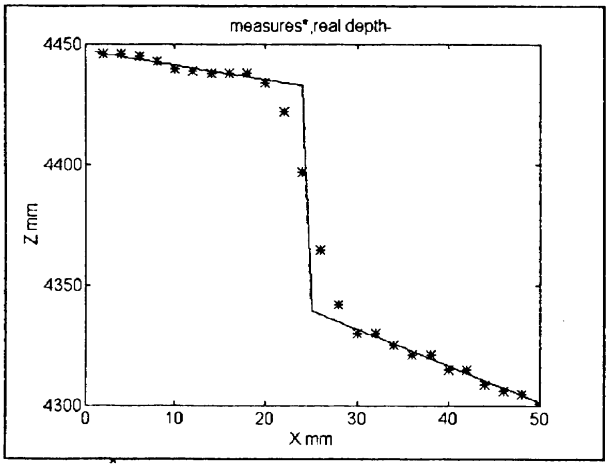

Fig. 10. Profile measured and real profile.

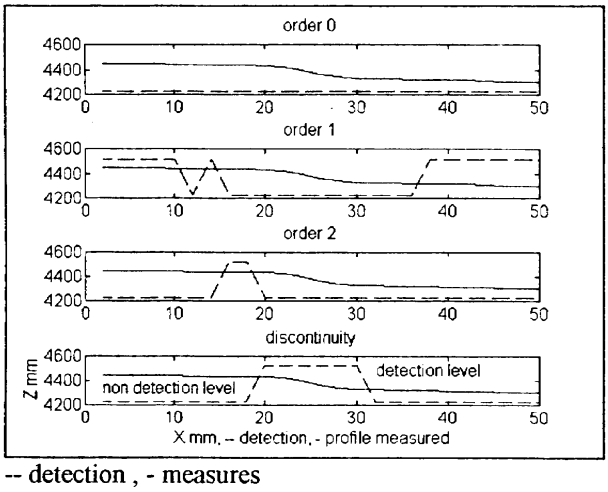

Fig. 11. Detection of profile classes.

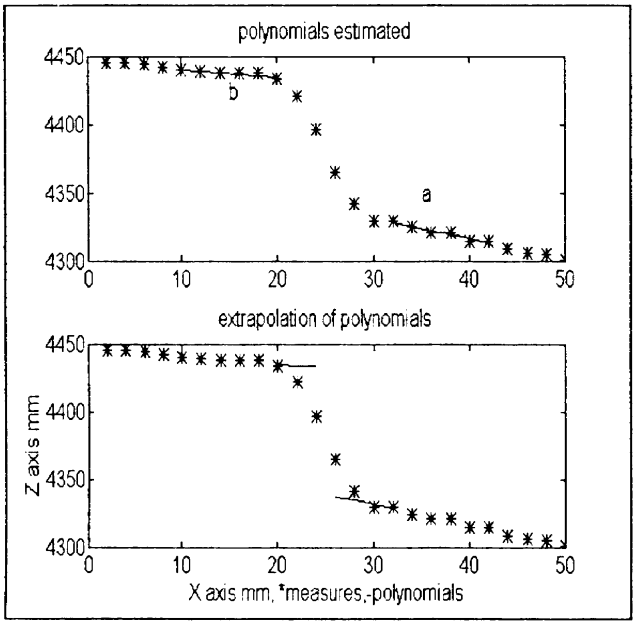

Fig. 12. Estimation-extrapolation of the polynomials.

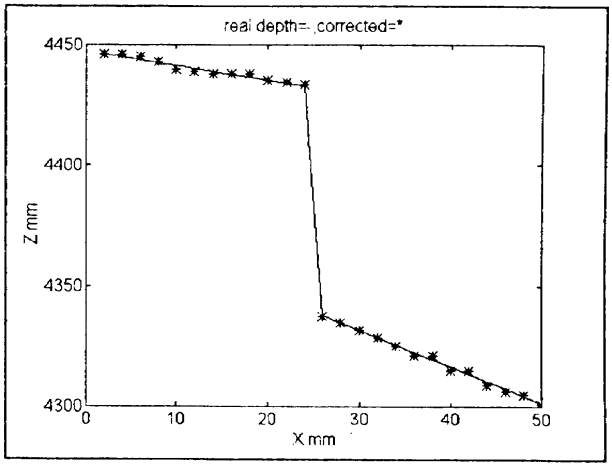

Fig. 13. Profile corrected.

building error related to the distance sensor-target of about 0.62% on z. The optimization method leads to a building error of about 0.35% on z and presents the advantage of computing both internal and external models.

As far as the range finder is concerned, the main objective is the improvement of the spatial resolution of the depth image. The physical limit is due to the diameter of the laser beam. The approach consists in treating the measures by a black box which acts as an inverse model. The inputs are a set of points belonging to a profile.

A NN-based solution is better than parametric methods. The problem is divided into a detection of the profile class by a NN and then a data correction by a parametric method.

These techniques can be spread over a depth image, line by line and column by column.

5. References

1. L. Trassoudaine, "Solution multisensorielle temps réel pour la détection d'obstacles sur route", *Thèse* (Clermont Ferrand, 1993).
2. C. Fröhlich, F. Freyberger and G. Schmidt, "A Three-dimensional Laser Range Camera for Sensing the Environment of a Mobile Robot" *Sensors and Actuators* 453–358 (1991).
3. Y. Cehkhar, E. Colle, A. Loukil and F. Chavand. "Multisensor calibration of a telerobotics aid system" *APII* **28,** No. 6, 599–623 (1994).
4. Y. Chekhar, "Saisie et traitement d'images télémétriques. Application à la téléopération" *Thèse* (Evry Val d'Essonne, 1994).
5. W.H. Press, S.A. Teukolsky, W.T. Vetterling and B.P. Flannery, *Numerical Recipes in C* (Cambridge University Press, Cambridge, Second Edition, 1992).
6. IBEO, Users guide (1992)
7. S. Guillon, "Caractérisation expérimentale et modèle simulé d'un télémètre LASER" *Thèse* (Paris XI, 1989).
8. S. Kitamura, "Neural networks and inverse problems in measurement and control", *Proc. IMACS/SICE International Symposium on Robotics, Mechatronics and Manufacturing Systems*'92 205–210, Kobe, Japan (Sept., 1992) pp. 205–210.
9. J.F. Jodouin, "Les réseaux de neurones" (Edition Hermès, 1994).

https://doi.org/10.1017/S0263574797000246 Published online by Cambridge University Press